Deep Resources Engineering 1 (2024) 100002

Contents lists available at ScienceDirect

Deep Resources Engineering

journal homepage: www.keaipublishing.com/en/journals/deepre/

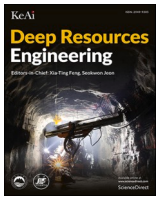

A novel DFN-DEM approach to simulate long-term behavior of crystalline rock under effects of glacial climate conditions

Friederike Tiedtke [a,*], Heinz Konietzky [a], Fabien Magri [b,c]

[a] Geotechnical Institute, TU Bergakademie Freiberg, Gustav-Zeuner-Str.1, 09599 Freiberg, Germany
[b] Division Research / International, Federal Office for the Safety of Nuclear Waste Management (BASE), Wegelystr. 8, 10623 Berlin, Germany
[c] Institute of Geological Sciences, Hydrogeology Group, Freie Universtität Berlin, 12249 Berlin, Germany

ARTICLE INFO

Keywords:
Nuclear safety
Numerical workflow
Geo-mechanical coupling
Fractures

ABSTRACT

The safety assessment of nuclear waste repositories is a critical yet challenging task. Several processes acting on different time scales and multiphysical couplings must be taken into account. The complexity of such assessments often requires integrating different software into a single numerical workflow. This study focuses on the long-term behavior of fractured rock masses and the alteration of the hydrogeological system under changing global climate conditions. The investigated impacts include the response of the rock mass due to heating of a generic repository, development of permafrost, and advance and retreat of an ice-shield. To represent THM processes on a timescale of ~100,000 years in crystalline rock, a novel DFN-DEM modelling approach has been developed. The modelling approach combines two numerical software tools. The thermomechanical calculations are carried out using the distinct element method (DEM) based tool 3DEC [1]. The flow field and the hydraulic heads in the fracture network are calculated with the DFN-tool DFN.Lab [2]. A proprietary script allows to couple and update parameters and variables that are needed to perform THM calculations linking the two different tools. The long-term THM simulations are tested on a generic model of crystalline rock that includes deterministic fault zones as well as a stochastic DFN as the key feature of the hydrogeological system. The modelling approach allows to analyze the behavior of the fracture network including fracture growth and the development of flow pathways within the fracture network as a response to the external THM impacts. The results of the simulations show that the superposition of the different THM processes favors the development of preferential flow pathways along large-scale faults during cold climate conditions.

1. Introduction

1.1. Aspects of the safety assessment for an underground repository

Evaluating the integrity of a potential host rock for a geological disposal of High Level radioactive Waste (HLW) is an important aspect in the safety assessment for an underground repository. For a regulatory authority like BASE, gaining insights into long-term physical processes in potential host rocks is of great importance to fulfill its role in providing expertise to supervise nuclear safety. In this regard, the project "AREHS" was conceived and developed to understand impacts of changing conditions (e.g., glacial cycles) on major host rocks (clay, salt and crystalline rocks). This study focuses on crystalline rocks.

During the lifetime of an underground repository, the natural barrier may be affected by external impacts and internal THM processes. In fractured rock mass, the fracture network is the key feature of the hydrogeological system [3–5]. Matrix flow in crystalline rock is often assumed to be negligible, usually fluid flow is concentrated in fractures [5–7]. As a result, the representation of complex fracture networks in numerical models is an important aspect to evaluate the effects of THM processes on the natural barrier. In addition to the complex physical processes in the geosphere, the different time scales on which these processes operate pose further challenges to numerical modelling for the safety assessment of an underground repository. The international institution "NEA" has systematically compiled a catalogue, that lists Features, Events and Processes (FEPs) with a potential hazardous impact for a nuclear waste repository [8]. In this study, FEPs are selected according to their relevant spatial and temporal scale. The focus of the

Peer review under responsibility of Editorial Board of Deep Resources Engineering.
* Corresponding author.
E-mail address: friederike.tiedtke@ifgt.tu-freiberg.de (F. Tiedtke).

https://doi.org/10.1016/j.deepre.2024.100002
Received 18 October 2023; Received in revised form 17 January 2024; Accepted 22 January 2024
Available online 11 March 2024

THM simulations is on *far-field* processes with *long-term* impacts. Therefore, three main impacts during the lifetime of a repository have been selected: thermal loading, permafrost and glaciation. These impacts generally represent the evolution of a repository and climate conditions over a period of about 100,000 years.

Thermal loading (FEP 3.2.1) occurs due to the heat released from waste inventory in the repository. The temperature rise can affect the stress field around the underground repository. Thermal stresses can develop not only in the near-field of the repository, but also reach far-field areas [9]. Due to the unconfined nature of the ground surface, surface heave can be caused by the thermal expansion of the rock [9,10]. Hoekmark et al. [10] report a heave of several centimeters in their linear-elastic large-scale model for the Forsmark repository lay-out. Thermal stresses are generated mainly in horizontal direction. In [11], a large-scale FEM model has shown increased horizontal compressive stresses at repository level and horizontal tensile stresses at the surface, which may favor fracturing processes. The response of the fracture network to the thermal induced stress perturbations is very complex and depends on in-situ stress-field and fracture orientation. Hoekmark et al. [10] derive from their large-scale thermomechanical simulations stress-dependent transmissivity changes. They report reduced transmissivities for most fractures and a modest transmissivity increase is observed in vertical fractures close to the surface. This heterogenous fracture behavior controlled by thermal compression, resulting in fracture closure, thermal induced shearing, as well as fracture opening due to dilation, is highlighted in [12]. Kwon et al. [12] analyze the thermomechanical behavior of a near-field model of Forsmark with an explicit DFN representation.

Permafrost (FEP 1.3.4) is defined as "ground (soil or rock and included ice or organic material) that remains at or below 0 °C for at least two consecutive years" [13]. Permafrost may influence the pattern of groundwater flow. In [14] permafrost is implemented as a zone with low hydraulic conductivity. Hoekmark et al. [10] present a reduction of the horizontal compressive stresses in the order of several Megapascals due to the cooling process at the ground surface. The alteration of the stress-field may lead to fracture opening. A transmissivity increase directly below an impermeable permafrost layer is derived as a result of the thermomechanical effects of permafrost conditions in [10].

Glaciation (FEP 1.3.5) describes the advance, stagnation and retreat of an ice-shield. In [15], the ice-shield is displayed as a mechanical load, which causes irreversible shear displacements in their large-scale 3DEC model of Olkiluoto. Kwon et al. [12] analyze fracture behavior under the influence of a mechanical ice-load in their near-field model of Forsmark. They observe an overall transmissivity increase, locally even an increase of several orders of magnitude. In [10] elevated pore pressures are considered in addition to the mechanical ice load. Their assumptions for the elevated pore pressures are obtained from 2D FEM simulations. The calculated pore pressure in [10] was adopted to act as the pressure within fractures in order to derive fracture shear strengths and transmissivities. They conclude that the pressure assumptions are crucial for the slip behavior of the fractures. In these studies, no analysis of flow pathways within fracture networks based on an explicit flow calculation is carried out.

The purely mechanical consideration of the ice-shield that is often used in numerical studies is a strong simplification of real glacial conditions. The thermal regime/condition at the glacier bed is significant for the mechanical and hydrogeological interaction with the geosphere. Ice creep and basal sliding can cause thawing of the underlying permafrost (= "warm-based" ice-shield), resulting in the alteration of the thermomechanical conditions [16]. Additional to the mechanical load, a key process associated with warm-based glaciers is the extensive infiltration of basal meltwater.

1.2. Scope and goals

The numerical model presented in this study approaches two main challenges not addressed in the above studies: 1.) the integration of an explicit representation of a fracture network as the main feature for fluid flow and, simultaneously, 2.) the modeling of THM processes on a timescale of 100,000 years to cover a complete glaciation cycle. To overcome these challenges, a combined DFN-DEM approach has been developed using the numerical software codes "3DEC" [1] and "DFN.Lab" [2].

The distinct element method (DEM) is a very accurate technique when it comes to simulate THM processes in fractured media. But due to its explicit algorithm and small timesteps, it is computational demanding, especially for the considered timespan.

Complex networks can be explicitly represented in 3D numerical models as a stochastic "Discrete Fracture Network" (DFN), where fractures are classically assumed to be disc- or polygonal shaped planar objects. The geometric properties (e.g., size, orientation, position) follow certain statistical distributions derived from field mapping. DFNs can act not only as a geometric description of fractured media, but also as a numerical model that solves fluid flow within connected fractures of the network [17]. Since the fractures are represented as N-1 dimensional objects in N-dimensional space, solving steady-state flow in DFNs is computationally efficient.

The idea of the workflow is to couple the computationally efficient DFN flow calculation in DFN.Lab with the already well-established explicit thermomechanical calculation for block interactions in 3DEC in order to create a computationally feasible numerical workflow.

The modelling workflow is explained in *Section 2* . The focus of this study is to identify changes in the hydrogeological system and the formation of preferential fluid pathways within the fracture network. Relevant processes that can have an impact on the geological barrier are analyzed. A generic rock mass model is generated consisting of deterministic fault zones as well as a stochastic DFN. The impacts considered are thermal loading, permafrost and glaciation. THM boundary conditions are used to reflect the key processes associated with an ice-shield cover. The geological model and the boundary conditions are described in *Section 3* . The results of the long-term THM simulation are presented in *Section 4* . A discussion of the results is given in *Section 5* .

2. Methodology

The numerical DEM code 3DEC is used for the thermal and mechanical calculations. 3DEC is a suitable tool to simulate the response of discontinuous (e.g. jointed) media to external and internal impacts. 3DEC can explicitly represent the joint network as "boundary conditions" to the surrounding matrix blocks. An explicit time-marching scheme is used to advance the block interaction. The mechanical interaction between blocks is governed by a contact model that is based on normal and shear stiffnesses to calculate the contact forces and displacements [4]. The flow calculations in the water bearing fracture network are carried out in DFN.Lab using a mixed-hybrid FEM approach [2,18].

The developed DFN-DEM approach is built around a sequential THM coupling scheme. In the first step of the THM calculation scheme, the changes in the temperature field due to the applied boundary conditions are calculated in 3DEC. Then, following the information transfer from 3DEC to DFN.Lab, flow within the fracture network is solved using DFN.Lab. The resulting fluid pressure field is imported into 3DEC. The mechanical response to the thermal, hydraulic and mechanical impacts on the rock mass is computed.

3DEC is an already well validated and verified tool for simulating the rock mass response to thermal, mechanical and hydraulic impacts [1]. Therefore, 3DEC is able to handle imported joint pressure fields correctly. A verification example for the flow solver in DFN.Lab is available on the developers' website [19].

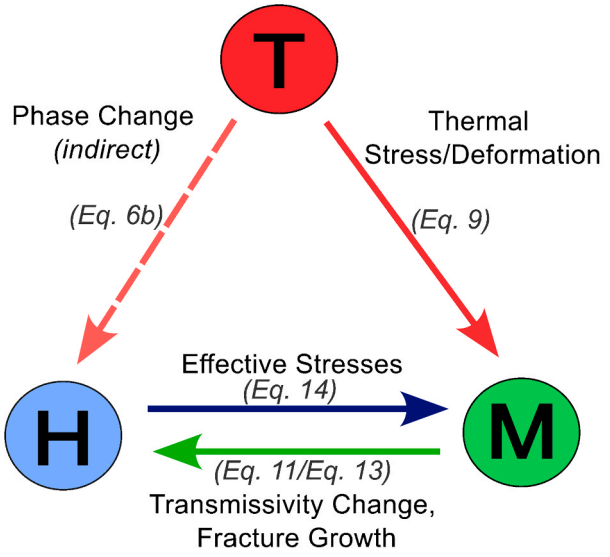

Fig. 1. Implemented THM Couplings: T → M: Changes in the temperature field induce thermal strains and stresses. T → H: Simplified approach to represent permafrost formation by reducing the fracture transmissivity at temperatures below 0 °C. H → M: Principle of effective stresses. M → H: Fracture normal displacements correspond to changes in transmissivity. Fracture growth is considered in the DFN flow calculation.

2.1. Governing equations

The implemented THM coupling is shown in Fig. 1. The heat transfer in the rock mass is governed by conduction. Convective heat transfer through the fracture flow is neglected since its influence on the temperature field is small compared to the conductive heat transport in the rock matrix for the spatial dimension and time scale considered in this study [20,21]. The Fourier law of heat conduction is applicable:

$$Q_i^T = -K_T \quad T_{,i} \tag{1}$$

where K_T is the thermal conductivity of the rock matrix and Q_i^T the heat flux vector. Additional heat as a result of deformation or friction is disregarded since the influence is assumed to be very small [20]. From Fourier's law (Eq.1) and the energy balance equation, the heat conduction equation can be written as:

$$\rho C \frac{\partial T}{\partial t} - K_T T_{,ii} = 0. \tag{2}$$

In order to be able to display a time period of 100,000 years, thermal mass scaling is used to raise the thermal timestep by several orders of magnitude. Further information regarding the mass scaling is provided by Itasca [1].

Under the assumption that the matrix flow in crystalline rock is negligible, only fluid flow in the (hydraulic active) fracture network is considered. The fracture flow is represented as flow between two parallel plates under the condition of laminar flow. The equation of conservation of flow (Eq. 3) and the Darcy Law (Eq. 4) are valid:

$$\left(Q_i^F\right)_{,i} = 0, \tag{3}$$

$$Q_i^F = -K_H \quad \phi_{,i} \tag{4}$$

where Q_i^F is the Darcy Flow vector, K_H is the hydraulic conductivity or "transmissivity" of the fracture and ϕ is the hydraulic head. The hydraulic head is related to the fluid pressure p inside the fracture as well as the geodetic elevation z (Eq. 5):

$$\phi = \frac{p}{\rho_f \quad g} + z \tag{5}$$

where ρ_f is the fluid density and g is the gravity. The "Cubic Law" (Eq. 6a) [22] quantifies the relationship between the hydraulic aperture u of the fracture (which here corresponds to the distance of the two parallel plates) and the fracture transmissivity b under consideration of fluid density ρ_f and fluid viscosity ν. A simplified approach to represent the formation of an impermeable permafrost layer is included in the numerical model by reducing the fracture transmissivity if the temperature T is below 0 °C (Eq. 6b). A pressure dependency of the ice-melting point is not considered.

$$b = \frac{u^3 \rho_f g}{12\nu}, T \geq 0 \tag{6a}$$

$$b = b_{\min}, T < 0 \tag{6b}$$

Due to the large time scale of the numerical simulation, it is assumed that the fracture network shows a fully drained response between two timesteps (~several years/decade) in the sequential THM calculation scheme.

For the deformable blocks, the constitutive equation of thermo-elasticity is valid. The total strain of a material point consists of two components: the mechanical strain caused by external forces and gravity and the thermal strain caused by the temperature gradients:

$$\varepsilon_{ij} = \varepsilon_{ij}^M + \varepsilon_{ij}^T \quad \text{Eq. (7)}$$

The elastic behavior can be quantified by Hooke's Law of elasticity:

$$\varepsilon_{ij}^M = \frac{1}{2G}\left(\sigma_{ij} - \frac{\lambda}{3\lambda + 2G}\delta_{ij}\sigma_{kk}\right) \tag{8}$$

where λ and G are Lamé 's elasticity constants and δ_{ij} is the Kronecker delta. The thermal strain is characterized by:

$$\varepsilon_{ij}^T = \alpha(T - T_0)\delta_{ij} \tag{9}$$

where α is the thermal expansion coefficient and $T - T_0$ is the difference between current and reference temperature.

The deformable (matrix) blocks are divided by the fracture network. The fracture planes/faults are represented as "contact planes" in 3DEC. A relation between contact stresses and relative displacements to describe the block interactions can in general form be written as:

$$\Delta\sigma_n = k_n \Delta u_n \tag{10a}$$

$$\Delta\sigma_s = k_s \Delta u_s \tag{10b}$$

where k_n and k_s are the normal and shear stiffnesses of the contact plane, and Δu_n and Δu_s are the relative displacements of the adjacent blocks. The Mohr-Coulomb constitutive model has been adopted to describe the joint behavior along the contact planes in 3DEC. The shear strength $\tau$is dependent on the effective normal stress σ'_n of the joint given by:

$$\tau = \sigma'_n \quad \tan(\varphi) + c \tag{11}$$

whereφ is the friction angle and c is the cohesion. After the shear strength is exceeded, dilation leads to additional fracture opening due to shear displacement (Eq. 12). This effect acts as long as the shear displacement is smaller than a predefined threshold value u_{cs} in order to prevent infinite joint opening.

$$\Delta u_{n-dilation} = \Delta u_s \tan(\psi), u_s < u_{cs} \tag{12}$$

where ψ is the dilation angle.

The effect of deformation on the fracture transmissivity displays the MH coupling. The change of the hydraulic aperture u corresponds to the

normal displacement:

$$u = u_0 + \Delta u_n \tag{13}$$

Fluid pressure in fractures influences the mechanical behavior of the fracture. Fluid pressure counteracts stress-induced fracture closing or may induce fracture opening or growth. The influence of the fluid pressure p is incorporated into the numerical model by using the principle of effective stresses:

$$\sigma'_n = \sigma_n + p \tag{14}$$

where σ'_n is the effective normal stress of the fracture and σ_n is the corresponding total stress.

2.2. Modelling workflow

The modelling workflow used for the simulation is sketched in Fig. 2. The basis of the modelling workflow is the generation and meshing of the 3DEC block model. An initial DFN consisting of planar, disc-shaped fractures is used to create the block geometries. The 3DEC block model consists of deformable blocks which are discretized in tetrahedral finite difference elements representing the rock matrix and their in between lying contact planes representing failure planes. The mechanical behavior on each contact plane is depicted by so-called "sub-contacts". The sub-contacts are grid points/vertices of the blocks' finite difference elements located on the contact plane. Sub-contacts store information of displacements and stresses acting on the contact planes. An indicator value for the current failure state is assigned to each sub-contact in 3DEC.

In this DFN-DEM approach, the sub-contacts on the contact planes are used for the information exchange between 3DEC and DFN.Lab. Since 3DEC prohibits the generation of partially fractured blocks, the contact planes extend to the associated block boundaries [1]. This means that sub-contacts inside the initial disc-shaped fracture geometry represent open fractures (i.e. state indicator = "failed") and sub-contacts outside the initial fracture geometry represent intact rock matrix (i.e. state indicator = "intact"). During the simulation, the stress state on contact planes will change. This may cause previously "intact" sub-contacts to fail if their assigned strength is exceeded. Based on sub-contact failure, the DFN geometry is updated for the flow calculation in DFN.Lab ("Contour Update", *Section 2.3*).

Once the 3DEC block model is built and the material properties for the rock matrix and contact planes are assigned, the simulation of the glaciation cycle is initiated. The THM calculation sequence starts with advancing one thermal timestep to compute the changes of the temperature field in 3DEC. Then, relevant sub-contact information is exported. A batch-file calls the DFN.Lab script to perform the hydraulic calculation. Based on the information from 3DEC, an updated version of the initial DFN is built, meaning that the fracture contours are adjusted according to sub-contact failure and the transmissivity field reflects the current normal displacements of the sub-contacts (Eq. 6a/6b) ("Transmissivity Update", *Section 2.4*). The updated DFN geometry is meshed and the transmissivity field is assigned as flow property. Hydraulic boundary conditions are applied and the steady-state flow within the DFN is solved. The resulting hydraulic head distribution in the DFN is used to update the fluid pressure in the 3DEC model ("Pressure Update", *Section 2.4*). Based on temperature field and fluid pressure, the mechanical calculation of the sequential THM scheme is carried out and the model is mechanically equilibrated. Then, the sequential THM calculation scheme starts again until the glaciation cycle is completed.

2.3. Contour update

To update fracture contours, only already failed sub-contacts are considered. Therefore, for each contact plane in 3DEC, the state indicator for each sub-contact is queried and the failed sub-contacts are filtered for the contour update. To account for fracture growth in the DFN model, it is assumed, that each fracture contour is described as the convex hull of all currently failed sub-contacts lying on the associated contact plane.

To determine the convex hull, the positions of these sub-contacts are utilized. Due to the planarity of the fractures, the search can be simplified to a 2D-spatial problem by transforming the 3D sub-contact point data using the fracture normal vector. The convex hull of the simplified 2D point data is determined by the QuickHull Algorithm [23] which is implemented in the open-source scientific computing library "Scipy" for the Python programming language [24].

Based on this spatial analysis of the failed sub-contacts, planar

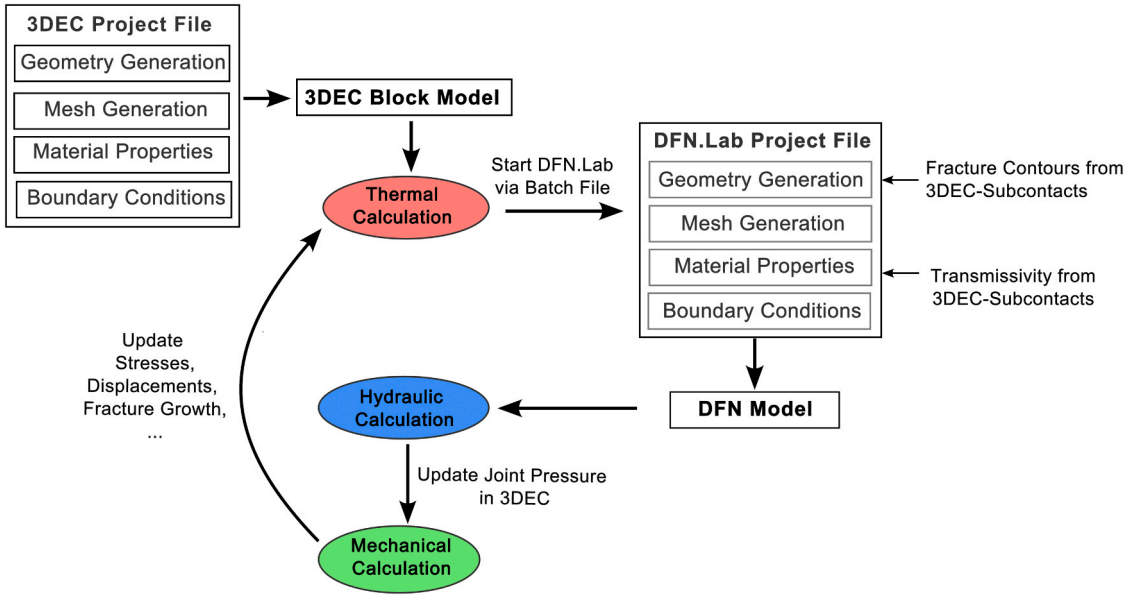

Fig. 2. Numerical workflow. The sequential THM calculation starts with the computation of the temperature field for the current timestep. After the thermal calculation is performed, the hydraulic calculation starts. The DFN.Lab script is called via a batch file and the DFN model based on the current sub-contact information is build. The results of the hydraulic calculation within the fracture network are used to update the fluid pressure in the 3DEC model. The mechanical response to the THM impacts is performed at the end of the sequence.

geometry objects are built, incorporating the new fracture contours for the updated DFN model.

2.4. Transfer of physical field variables

As the THM calculation scheme progresses, an information exchange between 3DEC and DFN.Lab is established. The relevant transfer variables are the normal displacement in order to update the transmissivity field in DFN.Lab and the hydraulic head distribution in order to update the fluid pressure in 3DEC. The transfer of those variables is based on 2D linear barycentric interpolation of unstructured point data, since the generated DFN.Lab and 3DEC meshes are spatially different. Here, again, the scientific computing library "Scipy" is used.

To update the transmissivity, the field variables are transferred from 3DEC to DFN.Lab. The normal displacement of the 3DEC sub-contacts is used to calculate the transmissivity according to Eq. 13 and Eq 6a. If the temperature of the sub-contact is below 0 °C, the transmissivity is reduced according to the simplified TH coupling (Eq. 6b). For each fracture, the sub-contact data of the transmissivity is interpolated on a 2D plane, utilizing the planarity of the fractures. Based on the interpolated data field, a transmissivity value is assigned as a property to each cell center in the DFN.Lab mesh used to solve steady-state flow.

The transfer of fluid pressure from DFN.Lab to 3DEC works analogously: The output of the flow calculation in DFN.Lab is the hydraulic head distribution within the fracture network. For each fracture, the hydraulic heads stored in the cell centers of the DFN.Lab mesh are converted to pressure values according to Eq. 5. The pressure values are interpolated on a 2D plane. The pressure value for each sub-contact is updated based on the interpolated pressure field.

3. Numerical model

In this study, the large-scale numerical model to demonstrate the simulation of a glaciation cycle using the presented DFN-DEM approach has a purely generic character. This means, that intentionally no specific site data regarding geology or material parameters were integrated. Nevertheless, the generated model reflects common properties of crystalline rock mass derived from various publications. The discussion will also address the generic character and implications for integrating site-specific information in the presented DFN-DEM workflow.

3.1. Generic discrete fracture model

A large-scale model is created to carry out the THM simulation of the glacial cycle. The model (10 km x 10 km x 3 km) displays a generic geological situation of crystalline rock. The outer model boundaries are aligned to the principal stress directions: The x-axis of the model is oriented N135°E, which corresponds to the direction of maximum horizontal stress in Europe. The y-axis is accordingly oriented in direction of the minimum horizontal stress.

In general, the geometrical properties (e.g., size, orientation, position) of discrete fracture networks follow certain statistical distributions ideally derived from field mapping. Extensive research has been conducted on the calibration of DFNs with stereological and hydrogeological field data to adjust network topography and transmissivity relations. Well-known examples for a systematic description of the fracture network are the geological disposal sites "Olkiluoto", Finland (e.g. [25,26]) and "Forsmark", Sweden (e.g. ([27–30]). Different approaches have been developed in order to further reproduce the complexity of fracture patterns found in field data [17]. A fracture network formation based on simplified mechanical rules ("nucleation, growth, and arrest") has been presented in [31]. The mechanical rules describe the phenomenon that large fractures stop the growth of smaller fractures. This approach has been further developed in [32].

As the literature review shows, the stereological description of rock mass is a complex and active field of research. To adjust DFN structures to site specific date, a comprehensive calibration process of the stereological and hydrological DFN parameters based on different field tests is necessary [26,29,30].

Based on general trends found in literature (e.g. [26,30,33]), the generic model used in this study should include a stochastic DFN as well as a set of deterministic fault zones. For the fault zones, it is assumed that there are two orthogonal-directed sets of fault zones (JS1 and JS2, Table 1), each with a spacing of 1 km. To connect the deterministic fault zones to the initial stress field (sect. 3.3), the strike directions of the fault zones align with the principal horizontal stress directions. A single, oblique fault (SF, Table 1) intersects the orthogonal fault network.

For the stochastic DFN, the following common properties for realistic DFNs have been derived from literature e.g. [30,33]:

- The orientations of the fractures in the DFN follow the Fisher-Distribution. Two main fracture sets are considered.
- A reduced fracture intensity with depth is targeted.
- A depth dependency of the transmissivity is embedded in a simplified form.

The stochastic DFN is implemented in the upper part of the model (Depth > - 1000 m) of the generic model, since this is the main area of interest. The fracture orientations in the stochastic DFN spread around the orientations of JS1 and JS2 (Fig. 3a). The minimum fracture length is set to 300 m and the maximum fracture length is 1000 m in the stochastic DFN. To implement the depth-dependencies in the stochastic DFN, three depth domains are specified. As an indicator for the fracture intensity, an (averaged) P_{10} – value is determined for each domain. The P_{10} – depth profile of the DFN is shown in Fig. 4. Based on the fracture center depth, a transmissivity value is assigned to the fracture (Fig. 4). The transmissivity of the DFN fractures ranges from 1e-8 m2/s to 1e-6 m2/s. The fault zones are assumed to be more conductive. The initial transmissivity of the fault zones is 1e-5 m2/s. To display the impermeable permafrost layer during the simulation, the transmissivity is reduced to 1e-13 m2/s if the temperature is below 0 °C.

The initial DFN geometry that is used to build the 3DEC block model contains only fracture clusters connected to hydraulic boundary conditions. Disconnected fractures and "dead-ends" are removed. In total, 19 faults and 191 fractures are generated for the generic fracture network model. The complete, hydraulically active DFN is shown in Fig. 3b.

3.2. Material properties

Material properties are derived from various sets of crystalline rock parameter reported in the literature [10,33,34] to represent generic behavior. The rock matrix behaves linearly elastic. The mechanical and thermal parameter set of the rock matrix is summarized in Table 2.

For the faults and fractures, the Mohr-Coulomb model is chosen. To avoid bad block geometries in the 3DEC model, horizontal geometry planes are generated with linear elastic behavior identical to the rock matrix. The parameter sets for the different joint types are shown in Table 3.

3.3. Initial conditions

The initial principal stresses act normal to the outer model boundaries. The initial stress field represents realistic conditions but does not include any site-specific stress data. The initial stresses in the numerical

Table 1
Main Fracture/Fault Zone Orientation.

	Strike [°]	Dip [°]
JS1	135	70
JS2	45	90
SF	160	90

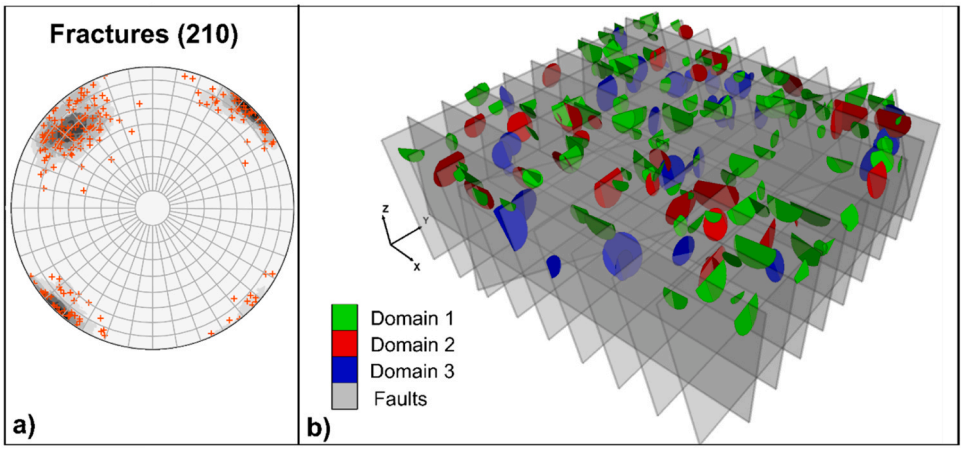

Fig. 3. a) Stereonet of the stochastic DFN in the upper part of the model. b) The generic DFN consisting of 19 fault zones (grey) and 191 fractures (colored) concentrated in the upper part of the model.

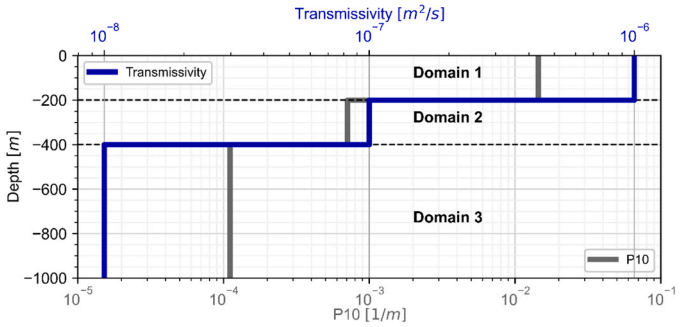

Fig. 4. Depth-dependency of the transmissivity in simplified form to represent generic but realistic flow conditions (blue). A transmissivity value is assigned based on the fracture center depth. The P10 depth profile (gray) shows a decreasing fracture intensity with depth for each domain.

Table 2
Rock Properties.

Density	E	Poisson's ratio	Conductivity	Specific Heat Capacity	Thermal Expansion Coefficient
[kg/m^3]	[Pa]	[-]	[W/(m K)]	[J/(kg K)]	[1/K]
2700	50e9	0.25	2.5	1000	7.5e-6

Table 3
Joint Plane Properties.

Property			Fault Zone	Fracture Plane	Geom. Plane
Normal Stiffness	k_n	[Pa/m]	60e9	600e9	1.2e9
Shear Stiffness	k_s	[Pa/m]	3e9	30e9	0.6e9
Friction Angle	φ	[°]	30	46*	
Friction Angle (res.)	φ_{res}	[°]	28	35	
Cohesion	c	[Pa]	0.2e6	19e6*	
Cohesion (res.)	c_{res}	[Pa]	0.1e6	0.4e6	
Tensile strength	t	[Pa]	0	1.5e6*	
Tensile strength (res.)	t_{res}	[Pa]	0	0	
Dilation angle	ψ	[°]	5	10	
Dilation threshold	u_{cs}	[m]	10e-3	10e-3	

* Represents intact rock

model are defined as:

$$\sigma_V = \rho_{rock} \times g \times z \tag{15}$$

$$\sigma_H = k_H \times \rho_{rock} \times g \times z - 5.297{*}10^6 \text{ , oriented } N135°\text{E} \quad \text{with } k_H = 1.6\ [-] \tag{16}$$

$$\sigma_h = k_h \times \rho_{rock} \times g \times z - 2.648{*}10^6 \quad \text{with } k_h = 0.8\ [-] \tag{17}$$

On the horizontal model boundaries, normal displacements are fixed, so that the model cannot expand horizontally. The bottom of the model is fixed.

Hydrostatic fluid pressure is initially assumed in the fault and fracture network. The hydrostatic pressure is fixed along the y-model boundaries. No flow boundary conditions are defined along the x-model boundaries and the bottom of the model.

$$P = \rho_{water} \times g \times z \tag{18}$$

The surface temperature is initially 8.5 °C. The geothermal gradient is 3 K/100 m. A geothermal flux of 70 mW/m^2 is applied at the bottom.

3.4. Boundary conditions

Based on the catalogue of relevant FEPs for the safety assessment by the NEA [8] thermal loading, permafrost and ice-load are selected as relevant impacts. The thermal loading starts immediately with the start of waste storage. Permafrost and ice-shield cover are associated with climatic conditions that differ greatly from present. conditions. This transition between interglacial and glacial climate conditions is divided into "episodes". Each episode describes a distinct external process, that significantly influences the geohydraulic system. An overview of the episodes is given in Fig. 5.

In the first episode (0–5,000 years), the thermal impact of the repository is considered. In the second episode (5,000–15,000 years), the warm climate conditions gradually change to cold climate conditions. The third episode (15,000–35,000 years) describes a period of periglacial conditions. The change from warm to cold climate conditions and the periglacial conditions are represent by (time-dependent) temperature boundary condition at the model surface. In the fourth (35,000–55,000 years), fifth (55,000–85,000 years) and sixth (85,000–95,000 years) episode, THM impacts due to ice-shield coverage (advance, stagnation and retreat) are considered. The boundary conditions are further specified in the following section.

3.4.1. Thermal loading

In the first episode, heat emitting from a generic repository acts as

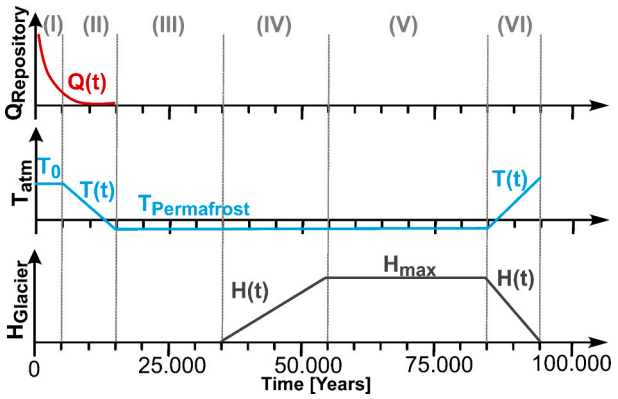

Fig. 5. Boundary conditions for the representation of the glaciation cycle. Ep. II: decrease of atmospheric temperature T_{atm}, Ep. III: minimum atmospheric temperature, Ep. IV: ice-shield advance, Ep. V: ice shield stagnation, Ep. VI ice-shield retreat. The ice-shield impacts are defined by the width and height of the glacier $H_{Glacier}$ according to the shape function (Eq. 19).
(a) The different THM impacts in the simulation sequence are the heat source Q, the atmospheric temperature T_{atm} and the height of the glacier $H_{Glacier}$. (b) I: heat source Q emitting from the repository, Ep.

thermal impact on the model. The generic repository is implemented as a smeared heat source at a depth of 500 m. In accordance to the German repository approach for crystalline rock, the area of the generic repository is divided into multiple effective containment zones. Therefore, four undisturbed model areas are selected from which heat will emit (Fig. 6). The four repository areas have a size of around 4 km^2 in total.

The exponentially decreasing heat source function presented in Jobmann et al. [35] is adopted. The total heat flux is generated by two different waste types ("BE" and "HA"). The heat properties of the two waste types are presented in [35]. The following assumptions are made regarding the heat evolution of the waste:

- "BE"-canisters were stored for 23 years before being emplaced in the repository. "HA"-canisters were stored 30 years before being emplaced in the repository [35].
- The waste storage is phased gradually over a time period of 80 years [35].
- In this study, the heat source is activated when waste storage is completed, which represents the peak of the heat source

The time-dependent heat source function used as boundary condition is shown in Fig. 7.

3.4.2. Permafrost

A linear decrease of the atmospheric temperature is modelled during episode II. The temperature at the model surface decreases linearly over a time interval of 10,000 years from initial 8.5 °C to − 1.5 °C. As soon as the lowest surface temperature T_{pf} is reached, the thermal boundary conditions are kept constant for a time interval of 20,000 years.

3.4.3. Glacial conditions

The glacier advance in episode IV starts after a long period of periglacial conditions. The development of a glacier is associated with complex physical impacts induced by two different thermal basal regimes, here referred to as "cold-based" and "warm-based". The thermal regime of an ice sheet is in reality spatially and temporally variable [13]. A simplified glacier model is reported in [16]: the central area of an ice shield is often cold-based due to very low air temperatures and a downward directed cooling by the accumulation of snow and firn. In the outer areas of a glacier under permafrost, strain and frictional heating induced by ice-creep and basal sliding can cause a change to "warm--based" conditions and result in a temperature inversion at the glacier bed. According to Dyke [16] the temperature inversion leads to melting of the underlying permafrost and infiltration of basal meltwater. The erosive capability of a warm-based glacier tends to be higher due to extensive basal meltwater [16]. To simulate the thermal impact of a "warm-based" glacier, the temperature inversion is simplified by setting the glacier basal temperature T_{GLC} to 0.5 °C. The time-dependent function for the glacier form is adopted from Bense and Person [36] (Eq. 19). The mechanical load of the glacier is the weight of the glacier, derived from the height function and the ice density $\rho_{ice} = 900$ kg/m^3. The infiltration of meltwater is modelled by defining hydraulic head boundary conditions. The hydraulic head at the glacier bed is 90% of the glacier height.

In episode IV, the time-dependent glacier advance/growth is simulated over a time interval of 20,000 years. In episode V, the maximum glacier extent is reached. For a time interval of 30,000 years, the glacier

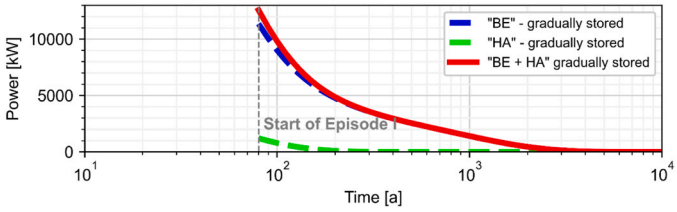

Fig. 7. Power function of the heat emitting waste. Total heat emitting from waste "BE" and "HA" after complete storage.

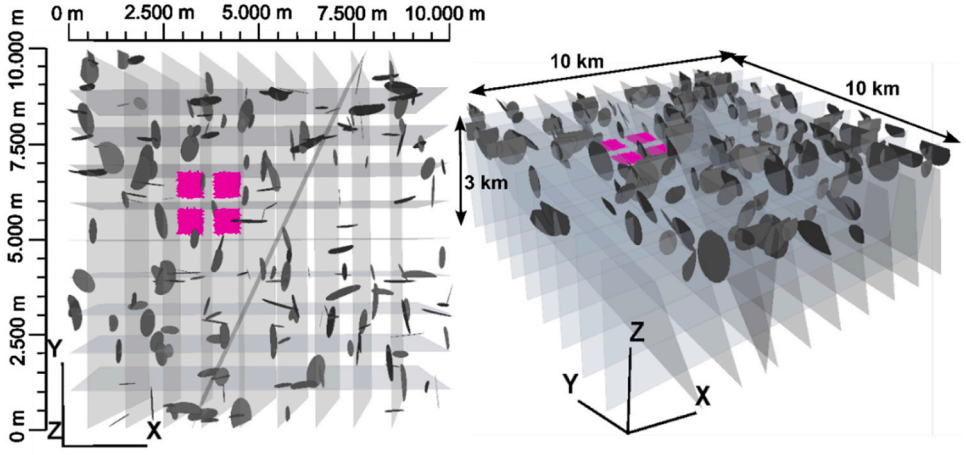

Fig. 6. Repository at a depth of 500 m represented as a smeared heat source located in four mostly undisturbed areas between the deterministic fault zones.

Table 4
Properties of the glacier. The form parameter "a" and "b" are adopted from Bense and Person [36].

L_{max}	H_{max}	x_0	a	b
Maximum Glacier Length	Maximum Glacier Height	Start Location of the glacier	Form parameter	Form parameter
8000 m	700 m	0 m	2.5	1.5

extent stays constant. In episode VI, the climate conditions start changing: The glacier retreats and simultaneously, the surface temperature rises linearly. The glacier advances and retreats in direction of the x-axis of the model.

$$h(t,x) = h_{\max}(t) \times ((1 - x_i^a)^b) \tag{19}$$

with $h_{\max}(t) = H_{\max} \times \frac{t - t_{start}}{t_{end} - t_{start}}$ and $x_i = \frac{x - x_0}{L_{\max} \times \frac{t - t_{start}}{t_{start} - t_{end}}}$.

4. Simulation results

The simulation is carried out with a 3DEC block model made of over 1.8 million mesh elements and around 700,000 sub-contacts. The DFN. Lab calculations are conducted on meshes with around 300,000 (2D) mesh elements.

4.1. Temperature field

The largest changes in the temperature field occur in episode I. In relation to the generic repository area, the initial heat flux emitted from the waste repository is 3.19 W/m^2. A maximum temperature of 61 °C is reached in the repository areas after about 500 years (Fig. 8a). The temperature increase is clearly visible in the vicinity of the generic repository areas. At the end of the first episode (after 5,000 years) the influence of the repository on the temperature field is still locally recognizable by increased temperatures around the repository areas (Fig. 8b).

In episodes II and III, periglacial climate conditions are simulated by reducing the temperature at the model surface. Based on the thermal conductivity of the rock matrix, the basal heat flux and the atmospheric temperature, a permafrost layer (temperature < 0 °C) develops to a depth of about 50 m. At repository depth, a minimum temperature of 18 °C is reached at the end of episode III (after 35,000 years). The temperature field at the end of episode III is shown in Fig. 9a. The perturbation of the temperature field around the repository areas due to the initial heating phase has subsided during the periglacial phase.

During episode IV, the permafrost beneath the advancing ice-shield starts thawing (Fig. 9b). In front of the glacier, the permafrost layer is still intact in episodes IV and V. In episode VI, the ice-shield retreat is accompanied by a rising atmospheric temperature. During episode VI, the temperature field approaches the initial state, but the disturbances caused by the periglacial and glacial conditions are still visible after the ice-shield retreat. At greater depths, the responses of the temperature field to the warming of the model are delayed. The temperature-depth profiles through the generic repository for different points in time during the long-term THM simulation are shown in Fig. 10.

4.2. Rock stresses and displacements

The vertical displacement fields during the heating phase of the generic repository are shown in Fig. 11. The increased temperatures in episode I cause an expansion of the rock matrix. The numerical model predicts a heave of about 9 cm for the unconfined model surface after 5,000 years. The temperature reduction in the periglacial episodes II and III leads (contrary to the behavior in episode I) to thermal contraction of the rock matrix. The thermal contraction causes a large-scale subsidence at the model surface up to 15 cm at the end of episode III (Fig. 12a). During the glaciation, the model is deformed in response to the glacier weight. Beneath the ice-shield, displacements in the order of 55 cm occur (Fig. 12b).

Profiles of the horizontal stresses through the generic repository for different points in time are shown in Fig. 13. Profiles of the stress ratios (σ_H/σ_v and σ_h/σ_v) through the generic repository for different points in time are shown in Fig. 14. Due to thermal expansion of the matrix in the vertical direction, compressive stresses are mainly induced in both horizontal directions in the vicinity of the repository (Fig. 13). An increase of about 10 MPa is observed at the repository level (t = 500 years). As a consequence, the ratio of the principal stress changes: The vertical stress is no longer acting as intermediate stress, but as minimal principle stress at the repository level of 500 m (Fig. 14). In contrast to the behavior around the repository, the uplift causes a decrease of horizontal compression close to the model surface. Under periglacial conditions (episode II and III), a decrease of the horizontal compression occurs as a result of thermal contraction of the rock matrix and the fixed model boundaries. At the model surface, a horizontal stress reduction of 4 MPa is predicted (t = 35,000 years). The initial generic stress field in combination with the boundary conditions therefore cause the

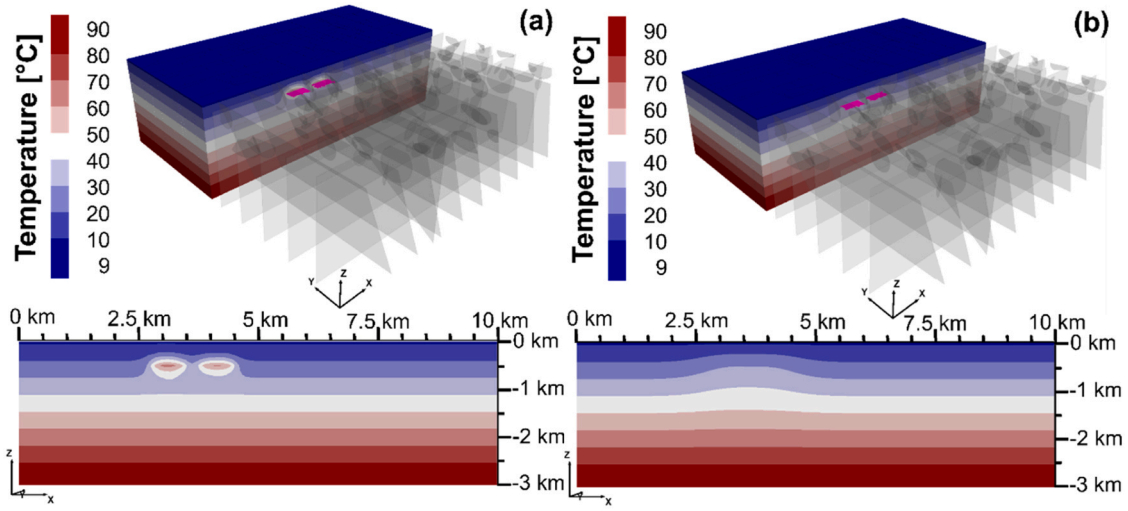

Fig. 8. (a) Temperature field [°C] in the cross-section of the repository (Y=5500 m) after 500 years. (b) Temperature field [°C] in the cross-section of the repository (Y=5500 m) after 5,000 years of repository heating. Even after 5000 years, the initial temperature conditions are not yet reached.

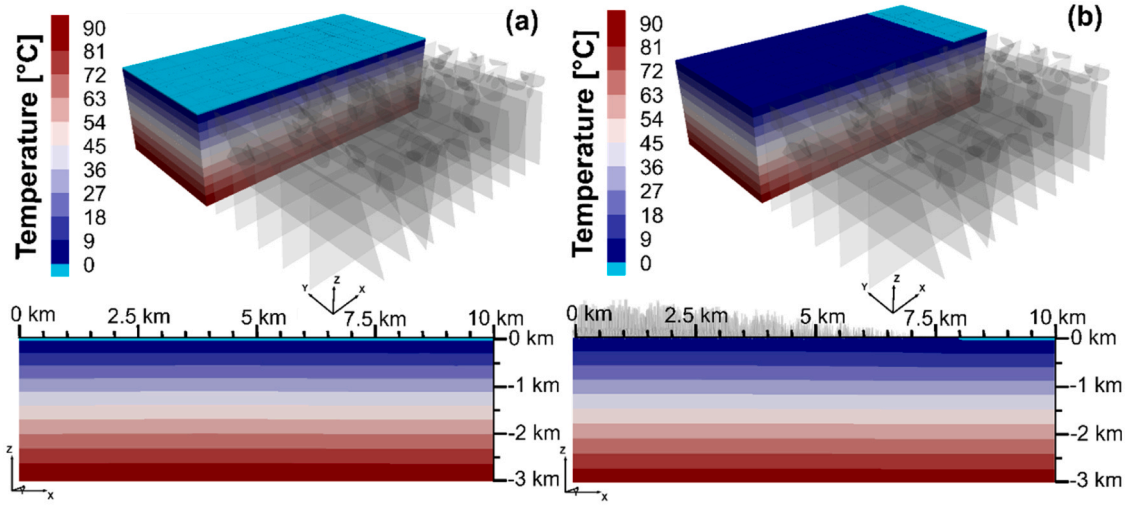

Fig. 9. (a) Temperature field [°C] in the cross-section of the repository (Y=5500 m) after 35,000 years. A permafrost layer (cyan) has developed to a depth of 50 m. (b) Temperature field [°C] in the cross-section of the repository (Y=5500 m). The temperature boundary condition of the glacier leads to thawing of underlying permafrost. After the glacial advance (55,000 years), permafrost is solely in front of the glacier.

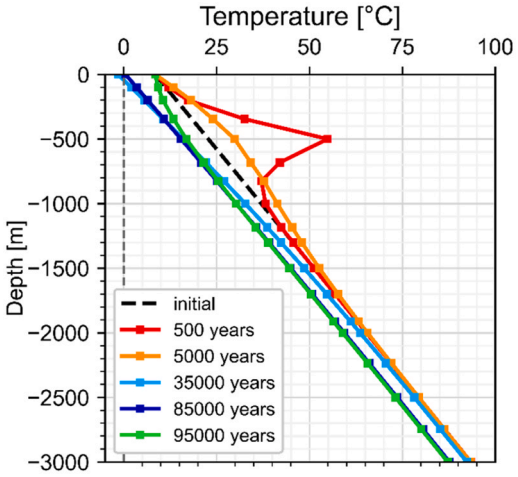

Fig. 10. Temperature-Depth Profiles (X = 4000 m, Y=5500 m): *500 years:* approx. time of the maximal repository temperature. A strong temperature disturbance is visible at the repository level *5,000 years*: end of episode I. The influence of the heat source is still visible. *35,000 years*: end of permafrost boundary conditions/episode III. A permafrost depth of 50 m has built up *85,000 years*: end of maximal glacier extent/episode V – close to the surface, the temperature increases as a result of the temperature boundary condition T_{GLC} of the glacier *95,000 years*: end of glacier retreat/episode VI. The thermal profile approaches the initial state.

formation of horizontal tensile stresses at the model surface. This effect is reversed in episode IV and V as the ice-shield loading increases the horizontal and vertical compression (t = 85,000 years). The increase of the horizontal compression is further enhanced by the temperature increase below the ice-shield and the accompanied re-expansion of the rock matrix. The depth profiles of the stress ratios show in the upper 200 m of the model values close to 1.0 (Fig. 14). Due to the periglacially influenced stress field and the previous decrease of horizontal compression, the thermomechanical effects of the ice-shield favor the development of an isotropic stress state close to the model surface.

4.3. Joint stresses

The response of the discontinuities to the different THM impacts and the corresponding changes in the stress field is very complex. To evaluate the stress changes in respect to potential failure on the fault zones in the vicinity to the repository, monitoring points are established. Monitoring points are located on fault #1 at X = 3500 m and Y= 5500 m, which is part of JS1, and on fault #8 at X = 3500 m and Y= 5000 m, belonging to JS2. Four different depths are evaluated for each fault zone. Fig. 15 shows normal and shear stresses acting on fault #1 (JS1) and Fig. 16 shows the stresses acting on fault #8 (JS2) at the end of every episode. It is visible in the stress evolution that periglacial and glacial conditions generally cause a decrease of the normal stresses due to their THM impacts. On fault #1, only the point at a depth of 50 m reaches its strength criterion due to the impact of the ice-shield. The mechanical load of the ice-shield increases the normal stress on the 70° dipping faults of JS1, therefore counteracting the increased fluid pressures beneath the ice-shield. On the contrary, JS2, perpendicular to the minimum horizontal stress direction, is more susceptible to failure. The failure of the points on fault #8 at a depth of 50 m and 150 m are caused by the significant stress reduction during the periglacial permafrost conditions. Ice-loading and the associated fluid pressure increase in the fracture and fault network below the ice-shield cause the strength criterion to be exceeded on fault #8 to a depth of 450 m.

Fracture growth of the DFN is also observed during the glaciation cycle, resulting in an increased connectivity within the network (Fig. 17). The thermomechanical induced fracturing during episode II and III are predominantly observed close to the surface (depth < -250 m).

4.4. Transmissivity evolution / fracture flow

During the thermal loading in episode I, two different mechanisms determine the transmissivity field. The thermal expansion around the repository leads to a normal closure of the adjacent vertical fault zones which belong to JS2. (Fig. 18a). This thermally induced transmissivity decrease is most pronounced at the peak temperature. On the 70° dipping fault zones of JS1, shear displacement accompanied by dilatational effects influences the transmissivity field. The closure effects of JS1 are therefore less dominant than in JS2. At the end of the thermal loading, transmissivity increase can be observed on the vertical faults close to the model surface (Fig. 18b).

The periglacial conditions in episode II and III result in a strongly heterogeneous transmissivity distribution along large-scale fault zones: The permafrost layer is assumed to be almost impermeable, therefore the transmissivity is reduced drastically (T = 1e-13 m^2/s). Beneath the permafrost, the thermal contraction of the matrix material causes an

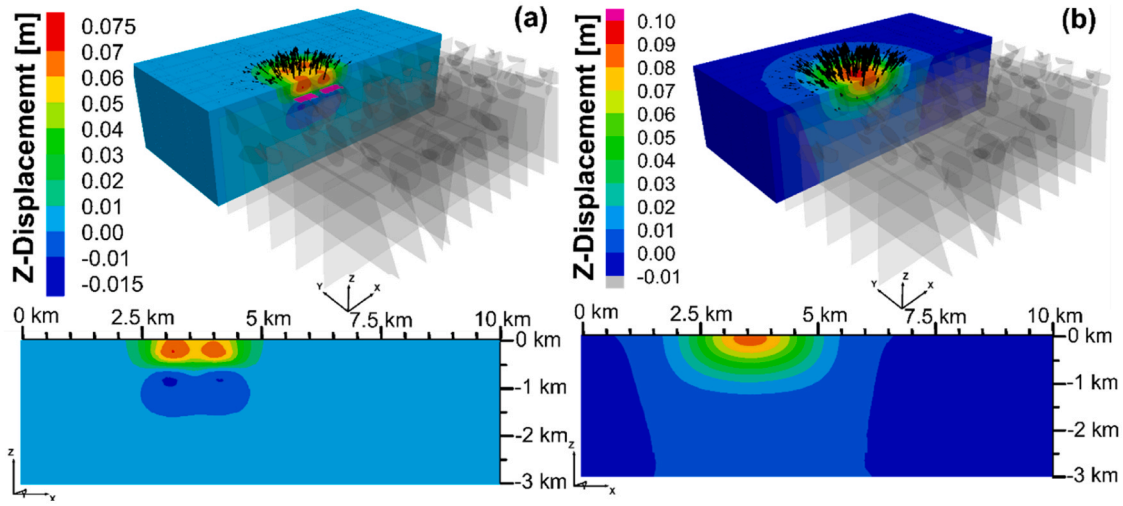

Fig. 11. a) Z-Displacement field [m] in the cross-section (Y=5500 m) of the repository after 500 years of repository heating; b) Z-Displacement field [m] in the cross-section (Y=5500 m) of the repository after 5000 years of repository heating. A surface heave of approximately 9 cm is predicted above the repository.

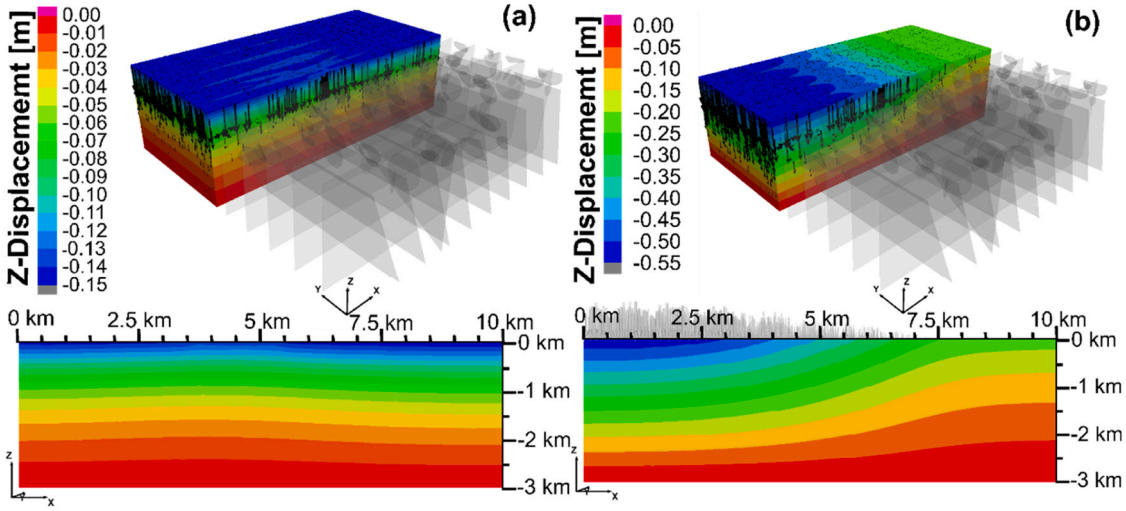

Fig. 12. a) Z-Displacement field [m] in the cross-section (Y=5500 m) of the repository after 35,000 years; b) Z-Displacement field [m] in the cross-section (Y=5500 m) of the repository at the end of the glacier advance (55,000 years). The displacement field reflects the glacier shape, i.e., ice-load. The glacier is depicted as applied force vectors (gray) at the model surface.

opening of the faults. The effect of temperature reduction becomes visible mainly on faults and fractures oriented normal to the minimum horizontal stress direction (Fig. 18c). As a result, the transmissivity field under periglacial conditions exhibits strong contrasts in hydraulic conductivity.

In addition to the thermomechanical impacts from the permafrost conditions, the ice-shield in episode IV-VI acts as a mechanical load and increases the hydraulic heads beneath it. The 70° dipping faults of JS1 start slipping due to the ice-load. The raised fluid pressures lead to further opening of the vertical faults belonging to JS2 (Fig. 18d). The superposition of these effects further increases the transmissivity in the network and enhances the formation of highly conductive zones.

Fig. 19 shows the evolution of the relative mean hydraulic aperture ($=u_{current}/u_{ini}$) for the fractures in the stochastic DFN. The repository does not affect the smaller fractures as much as the adjacent fault zones due to the fact that the repository is positioned in a predominately undisturbed area. At the end of episode III (t = 35,000 years), mean fracture apertures are decreasing close to the surface due to permafrost, but the trend of fracture opening caused by the thermomechanical stress reduction is also visible. During the glacial advance and stagnation (t = 85,000 years), the fractures mainly tend to open. The mean hydraulic aperture increases up to two orders of magnitude. During the glacier retreat (t = 95,000 years), the aperture partially recedes. That indicates that transmissivity changes in the fracture network partially trace back to irreversible shear-induced dilation. It is important to note, that the mean aperture only indicates general trends. However, the aperture distribution of a fracture is extremely heterogeneous.

Due to the pressure gradients, extensive basal meltwater infiltrates beneath the ice shield (Fig. 20). The high contrasts in transmissivity lead to a concentration of fluid flow in the highly conductive zones.

5. Discussion

Thermal expansion and contraction are the driving forces for the development of the transmissivity field. The transmissivity field is dependent on two main processes: reversible fracture normal closure/opening due to thermal expansion and contraction and irreversible fracture opening due to thermomechanical shear dilation.

The heat emitted by nuclear waste causes thermal expansion of the rock matrix. The thermal expansion is accompanied by an increase of

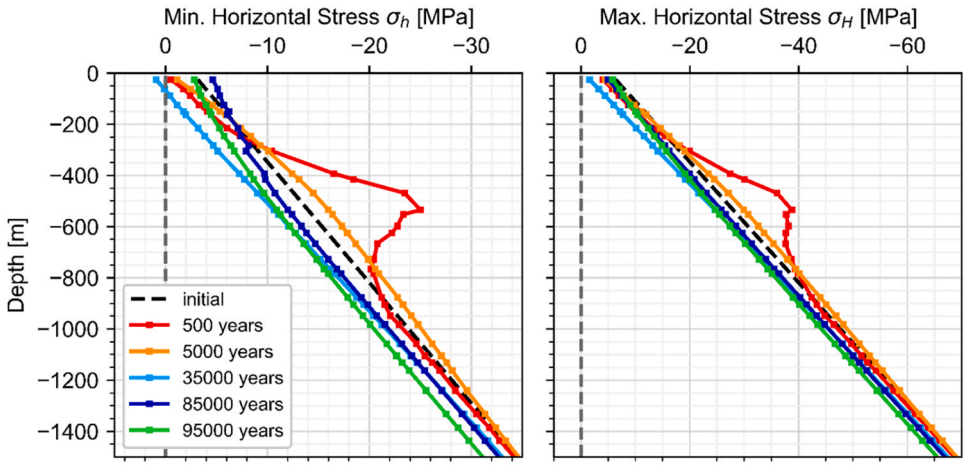

Fig. 13. Horizontal stress profiles. *500 years*: approx. time of the maximal repository temperature. An increase of compressive stresses is visible at repository level; *5,000 years*: end of episode I, the strong stress disturbance at repository level has receded; *35,000* years: end of episode III, a stress reduction is visible. The decrease of compression is most pronounced close to the surface; *85,000* years: end of episode V – additional compression due to the ice-shield loading; *95,000* years: end of episode VI – the ice-shield has retreated, stresses approach the initial state.

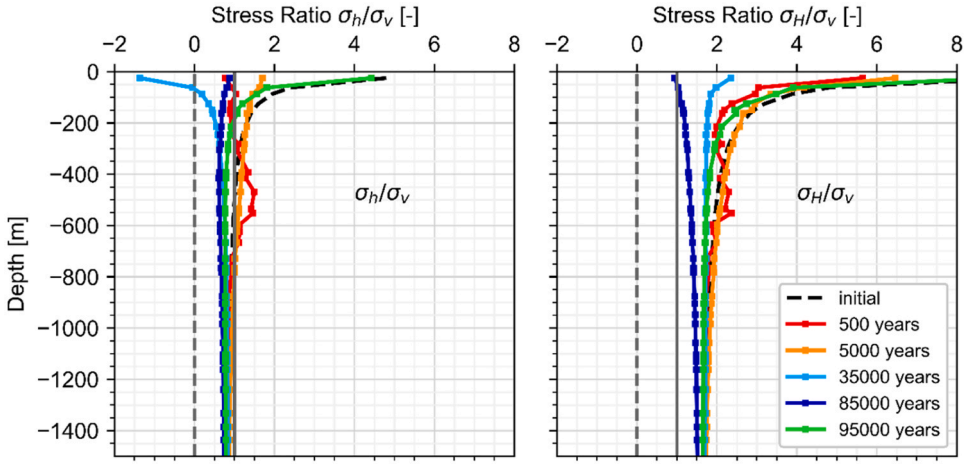

Fig. 14. Profiles of stress ratios: *500 years*: approx. time of the maximal repository temperature at repository level, the vertical stress becomes minimum principal stress at repository level; *5,000 years*: end of episode I; *35,000 years*: end of episode III – the contraction of the matrix caused by the periglacial thermal conditions favor in combination with the fixed boundary conditions a horizontal stress reduction; *85,000 years*: end of episode V; *95,000 years*: end of episode VI, stress ratios approach the initial state after the ice-shield retreat.

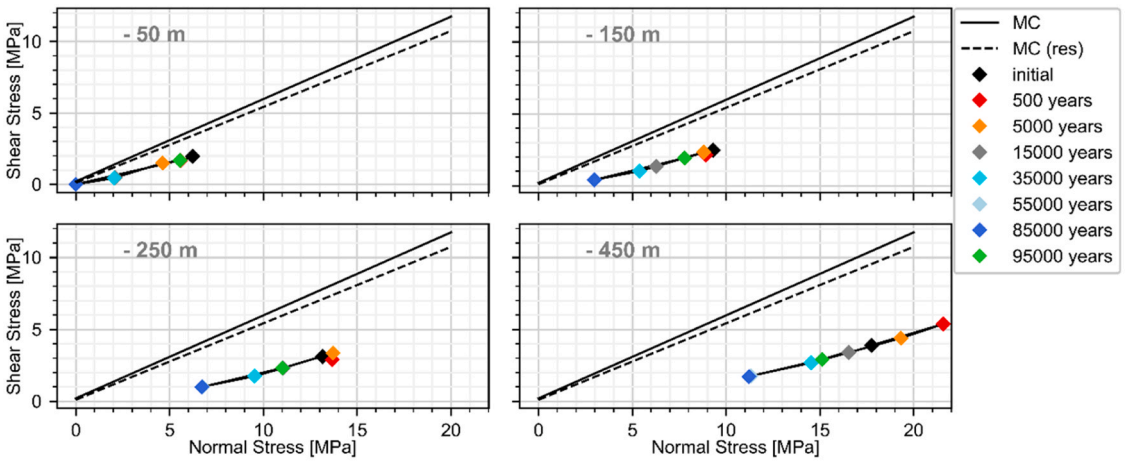

Fig. 15. Evaluation of the strength criterion at the end of every episode. Fault #1 reaches its strength criterion at a depth of 50 m as a result of the THM impacts during the ice-shield advance (Ep. IV).

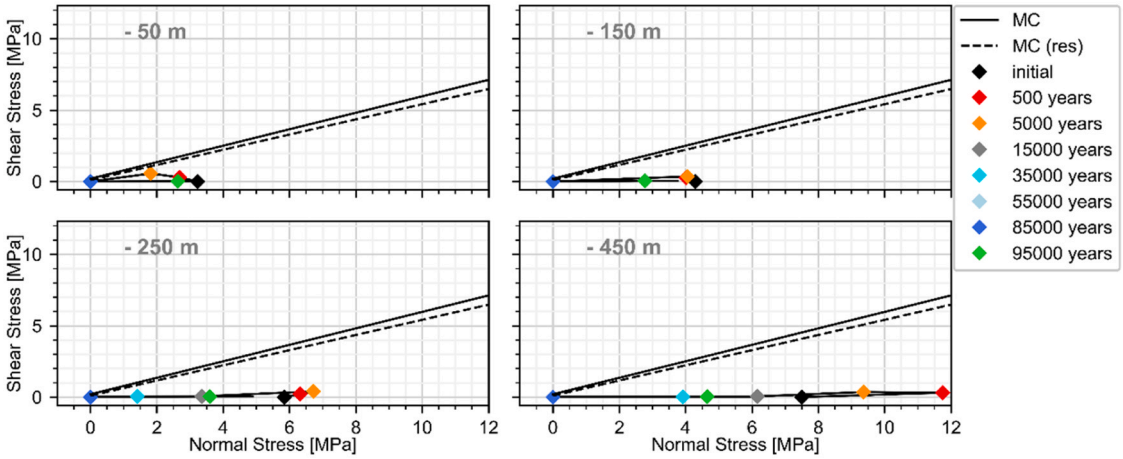

Fig. 16. Evaluation of the strength criterion at the end of every episode. For Fault #8, at depths of 50 m and 150 m the thermal induced stress reduction during permafrost conditions causes failure. The THM ice-shield impacts further enhance the normal stress reduction at depths of 250 m and 450 m.

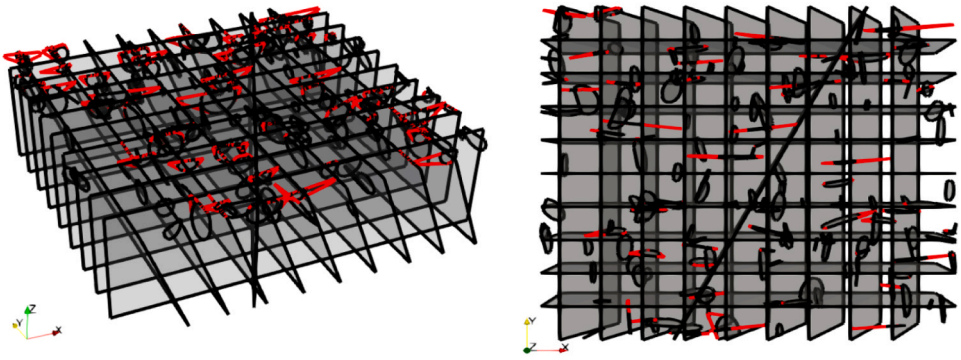

Fig. 17. Initial fracture network– black; updated fracture contours after periglacial conditions – red. As a result of the stress changes during the periglacial conditions, the interconnectivity between the different fractures/faults increases (predominantly close to the model surface).

horizontal compressive stresses at the repository level of around 10 MPa, and heave of 9 cm at the surface. In this simulation, the influence of the (reversible) normal displacement to decrease the transmissivity due to the additional horizontal compression dominates in the vicinity of the repository. After the first 5,000 years, shear-induced fracture opening caused by extensive heave exceeds the prior trend close to the surface.

The permafrost development has a strong influence on the stress field. Instability of the faults due to alteration of the stress field reaches a depth of around 250 m, depending on the orientation. Fracturing processes due to horizontal tensile stresses enhance the fracture network connectivity predominantly close to the surface. The thermal contraction of the material causes large-scale subsidence and can enhance the hydraulic conductivity below the impermeable permafrost region. The development of preferential flow pathways is favored due to high transmissivity contrasts. The quantitative impact is strongly dependent on permafrost depth, the strength of rock discontinuities (joints, faults), and the corresponding stiffnesses.

The fixed outer boundaries are a very conservative assumption for the evaluation of the thermomechanical processes especially during the thermal loading in episode I and the periglacial conditions in episode II and III in respect to the evolution of horizontal tensile stresses.

The processes of the ice-shield advance are very complex. The model response due to the boundary conditions shows large-scale displacements with maximum values of nearly 60 cm and an increase in transmissivity. The mean hydraulic aperture in the stochastic DFN increases by 2 orders of magnitude within a depth of 400 m. The induced fluid infiltration is strongly influenced by the previous alterations of the geohydraulic system. A superposition of thermal, mechanical and hydraulic model responses governs the fracture behavior. Partially, the fracture opening is reversible as Fig. 19 implies, but massive shear displacements are accompanied with the ice-load. The strength criterion of the faults parallel to the glacier advance is reached due to the elevated fluid pressure to depth of 450 m.

The long-term simulation of crystalline rock performed with the developed DFN-DEM approach shows reasonable results. The response of the rock mass to the different impacts in this study (repository heating, permafrost, ice-shield) is congruent with simulation results reported in literature [10–12]. In this respect, the proposed workflow for the THM coupled long-term simulations presented in this study can be considered as validated. The advantage of this workflow is the possibility to explicitly model the evolution of the fluid pressure and flow field within a growing fracture network to assess potential transport pathways.

Due to the generic nature of this study, assumptions were made regarding material properties, constitutive models, and the initial DFN geometry. To limit necessary input parameters for the generic rock mass model a simple joint constitutive model was selected. Of course, to represent the long-term response of the hydrogeological system, a detailed characterization of the shear behavior of the faults and fractures based on field observations is essential to distinguish which process dominates the development of the transmissivity field. The use of advanced constitutive models and consideration of temperature- and time-dependent material properties can further improve the simulations. Since aperture and fluid pressure act as coupling parameters in the workflow, the workflow itself is independent from selected constitutive

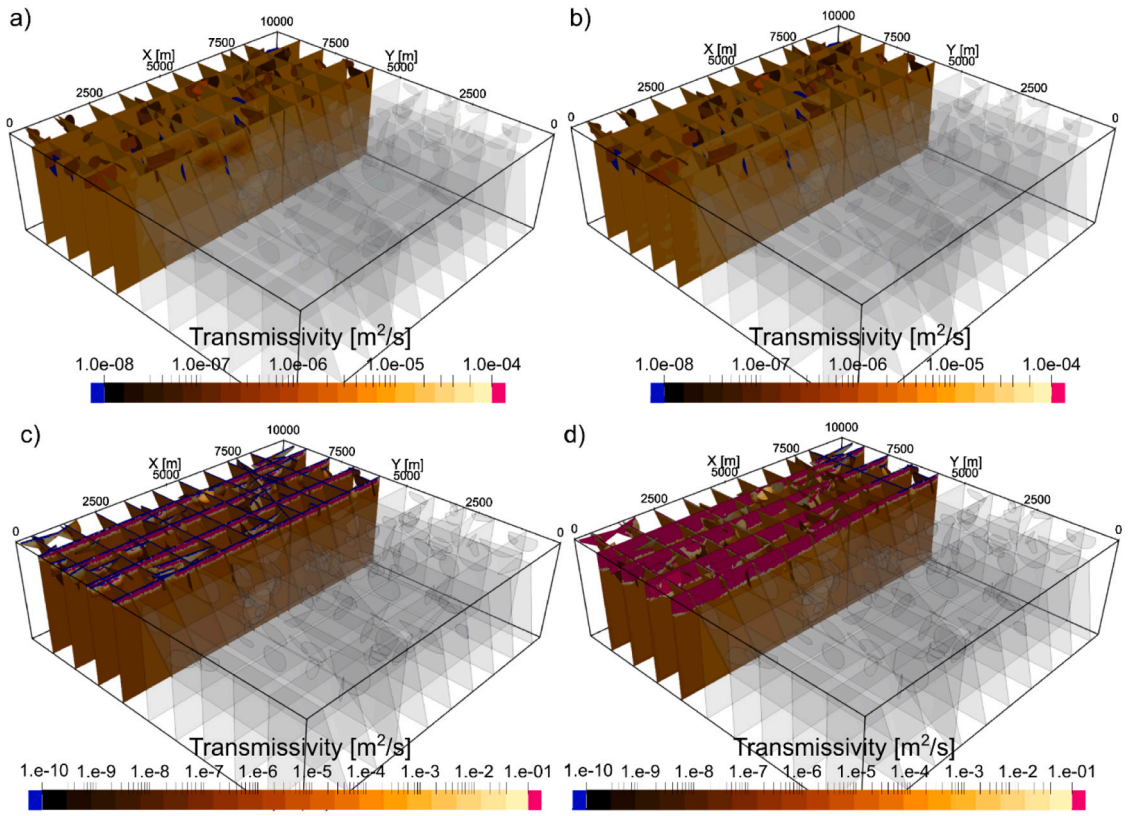

Fig. 18. Transmissivity evolution along the fault zone #8 adjacent to the generic repository. a.) Reversible closure caused by the heat source b.) Transmissivity increase close to the surface c.) Extremely high contrasts in transmissivity are developing due to the periglacial conditions d.) Ice-shield further enhances the transmissivity.

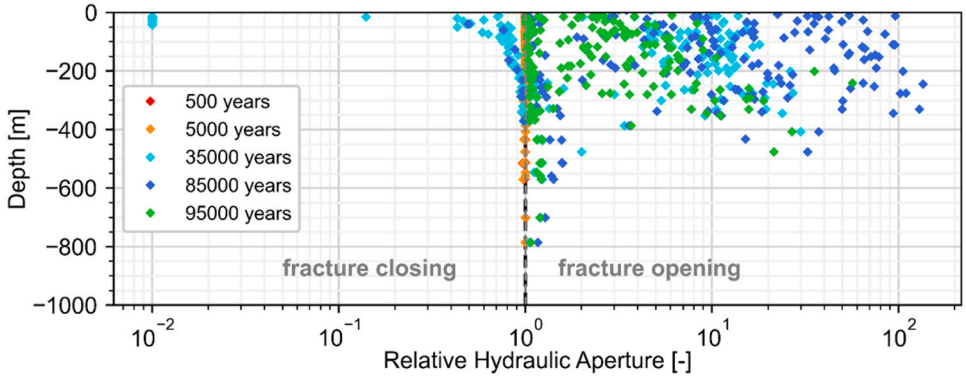

Fig. 19. Relative hydraulic aperture. Repository effects are not strongly pronounced, since the repository is positioned in an undisturbed area. Therefore, the thermal loading does primarily affect adjacent fault zones. A general trend of fracture opening during the periglacial and glacial conditions is visible. At a depth of 500 m, only minimal fracture opening is predicted, whereas at shallower depth an increase of the hydraulic aperture by 2 orders of magnitude strongly affects the hydrogeological system.

models, material properties or the initial DFN geometry. So, the assumptions made in this study are no limitations for the workflow. The well-established software "3DEC" is used to calculate the mechanical rock mass behavior, therefore different, more complex joint constitutive models that are already implemented in 3DEC can easily be selected to calculate the rock mass response.

The workflow is applicable to various geological settings of fractured rock masses. Different geological settings including a higher fracture density or additional fracture domains can be considered with the presented DFN-DEM workflow. The limiting factor for the workflow in regard to the DFN geometry is the possible mesh resolution and necessary block quality in 3DEC. The computational capabilities of 3DEC should not be exceeded by a potential geological model.

The assumption of a drained network response between two timesteps allows a timestep-independent solution of steady-state flow within a constantly updated fracture network. Due to the computational efficient flow calculations, the simulation with the propose DFN-DEM approach is not as time-consuming as classical DEM modelling. This assumption is justified by the relatively large timesteps (~decades) and the relatively slow loading velocity.

The non-consideration of undrained responses (e.g., hydraulic jacking) in the fracture network is a limitation of this workflow. As Hoekmark et al. [20] summarized, the prerequisite for hydraulic jacking to occur during glaciation in considerable depth are horizontal and

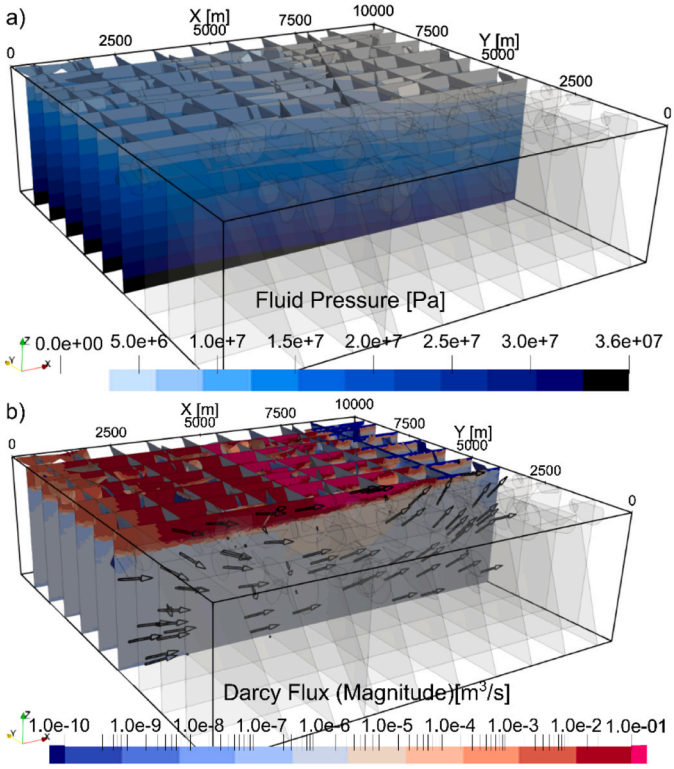

Fig. 20. Elevated fluid pressure in the fracture network as a result of the ice-shield cover b) Darcy flux in the fracture network. Fluid infiltration occurs beneath the ice-shield. Flow is concentrated in highly conductive areas. The black arrows indicate the flow direction.

subhorizontal connected fractures of great length transmitting hydraulic pressures over a large distance. Therefore, under specific geological conditions undrained processes should not be omitted.

Additionally, further improvement would be to adapt the workflow to non-planar fracture objects to create even more realistic fracture network geometries.

6. Conclusion

In this study, a THM workflow has been applied to model the behavior of a generic crystalline rock formation over a time span of 100,000 years. The workflow combines the DEM software 3DEC for thermal and mechanical calculations with the hydraulic calculation performed with the DFN-Software DFN.Lab. The “outsourcing” of the hydraulic calculation greatly improves calculation times compared to classical DEM simulations. The workflow therefore poses a feasible tool to simulate the long-term response of crystalline rock mass to THM impacts associated with glaciation.

For each episode, trends in the development of the hydrogeological system have been derived from a set of basic material properties for the crystalline rock. The general trends correspond well to trends reported in literature. The thermal loading due to heat emitting from a generic repository causes thermal expansion of the rock matrix and is accompanied by an increase of horizontal compressive stresses at repository level as well as heave movement above the repository. The transition to periglacial conditions causes a reduction of horizontal compressive stresses due to cooling of the rock mass. Fracture opening below an impermeable permafrost layer occurs. As a result, the hydrogeological system is governed by high transmissivity contrasts. This study considers ice-shield loading as THM impact. The superposition of the physical processes leads to failure processes along unfavorable oriented fault zones as well as enhancement of preferential flow paths.

The benefit of this workflow is the explicit representation of the fracture network and the consideration of fracture growth in the DFN flow calculations, which enables the analysis of preferential flow pathways and connectivity increase in the fracture network.

Declaration of Competing Interest

The authors declare that they have no known competing financial interests or personal relationships that could have appeared to influence the work reported in this paper.

Acknowledgements

This research is funded by the Federal Office for the Safety of Nuclear Waste Management under Grant No. 4719F10402 (AREHS project). Thanks to fruitful discussions and hints to improve the paper to Dr. Romain Le Goc (Fractory).

References

[1] Itasca Consulting Group, 3DEC - 3 dimensional distinct element code, Version 7.0., 2022, ⟨https://www.itascacg.com/software/3dec⟩, accessed 16 January 2024.
[2] R. Le Goc, B. Pinier, C. Darcel, E. Lavoine, D. Doolaeghe, S. De Simone, P. Davy, DFN. lab: software platform for Discrete Fracture Network models, Am. Geophys. Union Fall Meeting (2019) 2019.
[3] W.S. Dershowitz, H.H. Einstein, Three dimensional flow modeling in jointed rock masses, Proceedings 6th ISRM congress (1987).
[4] Lanru Jing, Ove Stephansson (Eds.), Fundamentals of Discrete Element Methods for Rock Engineering, Elsevier, 2007.
[5] K.-B. Min, L. Jing, O. Stephansson, Determining the equivalent permeability tensor for fractured rock masses using a stochastic REV approach: method and application to the field data from Sellafield, UK, Hydrogeol J. 12 (2004) 497–510, https://doi.org/10.1007/s10040-004-0331-7.
[6] J. Maillot, P. Davy, R. Le Goc, C. Darcel, J.R. de Dreuzy, Connectivity, permeability, and channeling in randomly distributed and kinematically defined discrete fracture network models, Water Res. Res. 52 (2016) 8526–8545, https://doi.org/10.1002/2016WR018973.
[7] M.R. Sweeney, J.D. Hyman, Stress effects on flow and transport in three-dimensional fracture networks, JGR Solid Earth 125 (2020) e2020JB019754, https://doi.org/10.1029/2020JB019754.
[8] M. Capouet, A. Carter, M. Ciambrella, International Features, Events and Processes (IFEP) List for the Deep Geological Disposal of Radioactive Waste, Version 3.0. OCED-NEA, Report No. NEA-RWM-R-2019–1., Paris, 2019.
[9] K.-B. Min, J. Rutqvist, C.-F. Tsang, L. Jing, Thermally induced mechanical and permeability changes around a nuclear waste repository—a far-field study based on equivalent properties determined by a discrete approach, Int. J. Rock Mech. Min. Sci. 42 (2005) 765–780, https://doi.org/10.1016/j.ijrmms.2005.03.014.
[10] H. Hoekmark, M. Loennqvist, B. Faelth, THM-issues in repository rock. Thermal, mechanical, thermo-mechanical and hydro-mechanical evolution of the rock at the Forsmark and Laxemar sites. SKB Technical Report TR-10–23, Stockholm, Sweden, 2010.
[11] K.-B. Min, J. Lee, O. Stephansson, Implications of thermally-induced fracture slip and permeability change on the long-term performance of a deep geological repository, Int. J. Rock Mech. Min. Sci. 61 (2013) 275–288, https://doi.org/10.1016/j.ijrmms.2013.03.009.
[12] S. Kwon, K.-B. Min, Fracture transmissivity evolution around the geological repository of nuclear waste caused by the excavation damage zone, thermoshearing and glaciation, Int. J Rock Mech Min Sci. 137 (2021) 104554, https://doi.org/10.1016/j.ijrmms.2020.104554.
[13] R.I. Waller, J.B. Murton, L. Kristensen, Glacier–permafrost interactions: processes, products and glaciological implications, Sediment. Geol. 255-256 (2012) 1–28, https://doi.org/10.1016/j.sedgeo.2012.02.005.
[14] R. Walsh, J. Alvis, Glaciation scenario: Groundwater and radionuclide transport studies. NWMO Technical Report TR-2010–09, Toronto, Canada, 2010.
[15] K.-L. Hutri, J. Anitkainen, Modelling of the bedrock response to glacial loading at the Olkiluoto site, Finland, Eng. Geol. 67 (2002) 39–49, https://doi.org/10.1016/S0013-7952(02)00108-4.
[16] A.S. Dyke, Landscapes of cold-centred Late Wisconsinan ice caps, Arctic Canada, Progress in Physical Geography: Earth and Environ. 17 (1993) 223–247, https://doi.org/10.1177/030913339301700208.
[17] Q. Lei, J.-P. Latham, C.-F. Tsang, The use of discrete fracture networks for modelling coupled geomechanical and hydrological behaviour of fractured rocks, Comput. Geotech. 85 (2017) 151–176, https://doi.org/10.1016/j.compgeo.2016.12.024.
[18] J. Maryška, O. Severýn, M. Vohralík, Numerical simulation of fracture flow with a mixed-hybrid FEM stochastic discrete fracture network model, Compu.t Geosci. 8 (2005) 217–234, https://doi.org/10.1007/s10596-005-0152-3.
[19] Fractory, DFN.Lab - A Software Platform for DFN Modelling, https://fractorylab.org/, accessed 16 January 2024.

[20] H. Hoekmark, B. Faelth, T. Wallroth, T-H-M couplings in rock. Overview of results of importance to the SR-Can safety assessment. SKB Technical Report R-06–88, Stockholm, Sweden, 2006.
[21] J.A. Hudson, O. Stephansson, J. Andersson, Guidance on numerical modelling of thermo-hydro-mechanical coupled processes for performance assessment of radioactive waste repositories, Int. J. Rock Mech. Min. Sci. 42 (2005) 850–870, https://doi.org/10.1016/j.ijrmms.2005.03.018.
[22] P.A. Witherspoon, J.S.Y. Wang, K. Iwai, J.E. Gale, Validity of cubic law for fluid flow in a deformable rock fracture, Water Resour. Res. 16 (1980) 1016–1024, https://doi.org/10.1029/WR016i006p01016.
[23] C.B. Barber, D.P. Dobkin, H. Huhdanpaa, The quickhull algorithm for convex hulls, ACM Trans. Math. Softw. 22 (1996) 469–483, https://doi.org/10.1145/235815.235821.
[24] P. Virtanen, R. Gommers, T.E. Oliphant, M. Haberland, T. Reddy, D. Cournapeau, E. Burovski, P. Peterson, W. Weckesser, J. Bright, S.J. van der Walt, M. Brett, J. Wilson, K.J. Millman, N. Mayorov, A.R.J. Nelson, E. Jones, R. Kern, E. Larson, C. J. Carey, İ. Polat, Y. Feng, E.W. Moore, J. VanderPlas, D. Laxalde, J. Perktold, R. Cimrman, I. Henriksen, E.A. Quintero, C.R. Harris, A.M. Archibald, A.H. Ribeiro, F. Pedregosa, P. van Mulbregt, SciPy 1.0: fundamental algorithms for scientific computing in Python, Nature methods 17 (2020) 261–272, https://doi.org/10.1038/s41592-019-0686-2.
[25] A. Buoro, K. Dahlbo, L. Wiren, Holmen Johan, Hermanson Jan, A. Fox, Geological discrete-fracture network model (version 1) for the Olkiluoto site, Finland. Posiva Oy Technical Report 2009-77, Finland (2009).
[26] L. Hartley, S. Baxter, A. Fox, A. Poteri, J. Suikkanen, Status and Outline Planning Report for Discrete Fracture Network Concepts, Data, Methods and Models for the Olkiluoto Site 2015. Posiva Oy Technical Report 2016–21., Finland, 2018.
[27] C. Darcel, P. Davy, O. Bour, J.R. de Dreuzy, Discrete fracture network for the Forsmark site. SKB Technical Report R-06–79., Stockholm, Sweden, 2006.
[28] C. Darcel, R. Le Goc, P. Davy, Development of the statistical fracture domain methodology–application to the Forsmark site. SKB Technical Report R-13–54., Stockholm, Sweden.
[29] C. Darcel, P. Davy, R. Le Goc, Statistical Fracture Domain Methodology For DFN Modeling Applied to Site Characterization., in: ISRM International Symposium - EUROCK 2012, OnePetro, 2012.
[30] S. Follin, L. Hartley, I. Rhén, P. Jackson, S. Joyce, D. Roberts, B. Swift, A methodology to constrain the parameters of a hydrogeological discrete fracture network model for sparsely fractured crystalline rock, exemplified by data from the proposed high-level nuclear waste repository site at Forsmark, Sweden, Hydrogeol J. 22 (2014) 313–331, https://doi.org/10.1007/s10040-013-1080-2.
[31] P. Davy, R. Le Goc, C. Darcel, A model of fracture nucleation, growth and arrest, and consequences for fracture density and scaling, JGR Solid Earth 118 (2013) 1393–1407, https://doi.org/10.1002/jgrb.50120.
[32] E. Lavoine, P. Davy, C. Darcel, R. Munier, A discrete fracture network model with stress-driven nucleation: impact on clustering, connectivity, and topology, Front. Phys. 8 (2020) 9, https://doi.org/10.3389/fphy.2020.00009.
[33] D.-A. Becker , N. Bertrams , R. Eickemeier , J. Flügge , B. Frenzel , J. Maßmann , K.-M. Mayer , J. Mönig , S. Mrugalla , N. Müller-Hoeppe , K. Reinhold , A. Rübel , N. Schubarth-Engelschall , E. Simo , J. Thiedau , T. Thiemeyer , J.R. Weber , J. Wolf , W. Bollingerfehr , RESUS - Grundlagen zur Bewertung eines Endlagersystems in einer Kristallingesteinsformation mit mehreren einschlusswirksamen Gebirgsbereichen. (Technical Report, in German) GRS-574, Gesellschaft für Anlagen- und Reaktorsicherheit (GRS) gGmbH, Cologne, Germany, 2020.
[34] X. Rachez, S. Gentier, 3D-hydromechanical Behavior of a Stimulated Fractured Rock Mass, in: Proceedings World Geothermal Congress 2010, Bali, Indonesia, 2010, 8 p. ⟨https://hal-brgm.archives-ouvertes.fr/hal-00495020⟩.
[35] M. Jobmann, V. Burlaka, P. Herold, E.K. Simo, J. Maßmann, A. Meleshyn, A. Rübel, G. Ziefle, Projekt ANSICHT Systemanalyse für die Endlagerstandortmodelle Methode und exemplarische Berechnungen zum Sicherheitsnachweis. (Technical Report, in German) TEC-29–2016-AB, BGR, 2017.
[36] V.F. Bense, M.A. Person, Transient hydrodynamics within intercratonic sedimentary basins during glacial cycles, F04005, J. Geophys. Res. 113 (2008), https://doi.org/10.1029/2007JF000969.

Friederike Tiedtke (Dipl.-Ing.) obtained her diploma degree in Geotechnical Engineering from TU Bergakademie Freiberg, Germany in 2020. She is currently a doctoral researcher at the Chair of Rock Mechanics at the same university. Her research interests are fracture representation in numerical models and multiphysical coupling in fractured rock mass. Her current work focuses on the development of efficient numerical workflows to simulate long-term rock mass behavior in the context of nuclear waste disposal.

Prof. Dr. Heinz Konietzky holds the esteemed position of a tenured professor and served many years as the head of the Institute of Geotechnical Engineering at TU Bergakademie Freiberg, Germany. His accolades include receiving the ISRM Franklin Lecture Award, chairing the Education Committee of FedIGES, and being a senior consultant for the globally recognized geotechnical software company ITASCA. Additionally, he is a member of the Czech Academy of Sciences evaluation committee, appointed expert for several mining authorities in Germany and Austria, member of the expert group for the Nuclear Inspectorate Switzerland ENSI and an editorial board member for esteemed international geotechnical journals like "Rock Mechanics and Rock Engineering" and "Journal of Rock Mechanics and Geotechnical Engineering." Prof. Konietzky's international influence is underscored by more than 200 published academic papers and leadership or participation in over 40 large-scale European and international collaborative projects. Having mentored eight Humboldt scholars from around the world, his innovative breakthroughs and outstanding contributions span diverse fields, including numerical computation, rock mechanics, and geotechnical engineering as well as material sciences and process engineering.